Versão do arquivo anexado / Version of attached file:

Versão do Editor / Published Version

Mais informações no site da editora / Further information on publisher's website:

https://www.hindawi.com/journals/ijce/2015/259603/

DOI: 10.1155/2015/259603

Direitos autorais / Publisher's copyright statement:

Research Article

Analysis of Process Variables via CFD to Evaluate the Performance of a FCC Riser

H. C. Alvarez-Castro,[1] E. M. Matos,[1] M. Mori,[1] W. Martignoni,[2] and R. Ocone[3]

[1]*School of Chemical Engineering, University of Campinas, 500 Albert Einstein Avenida, 13083-970 Campinas, SP, Brazil*
[2]*PETROBRAS/AB-RE/TR/OT, 65 República do Chile Avenida, 20031-912 Rio de Janeiro, RJ, Brazil*
[3]*Chemical Engineering, Heriot-Watt University, Edinburgh EH144AS, UK*

Correspondence should be addressed to M. Mori; mori@feq.unicamp.br

Feedstock conversion and yield products are studied through a 3D model simulating the main reactor of the fluid catalytic cracking (FCC) process. Computational fluid dynamic (CFD) is used with Eulerian-Eulerian approach to predict the fluid catalytic cracking behavior. The model considers 12 lumps with catalyst deactivation by coke and poisoning by alkaline nitrides and polycyclic aromatic adsorption to estimate the kinetic behavior which, starting from a given feedstock, produces several cracking products. Different feedstock compositions are considered. The model is compared with sampling data at industrial operation conditions. The simulation model is able to represent accurately the products behavior for the different operating conditions considered. All the conditions considered were solved using a solver ANSYS CFX 14.0. The different operation process variables and hydrodynamic effects of the industrial riser of a fluid catalytic cracking (FCC) are evaluated. Predictions from the model are shown and comparison with experimental conversion and yields products are presented; recommendations are drawn to establish the conditions to obtain higher product yields in the industrial process.

1. Introduction

Since the first FCC commercial riser, many improvements have been achieved which have helped the process reliability and its capacity to transform heavier feedstock at relatively low costs; currently the FCC process remains the primary conversion process in the petrochemical industry. For a number of refineries, the fluid catalytic cracking remains the main source of profitability and the accomplishment of its operation decides the market competiveness of the cracking unit. Approximately 350 FCC units are in operation worldwide, with over 12.7 million barrels per day as total capacity. Most of the existing cracker units have been designed or modified by six major technology licensers [1].

The design of each FCC unit can be different but their common target is to upgrade low-cost hydrocarbons to more valuable products. FCC and ancillary units, such as the alkylation unit, are responsible for about 45% of the gasoline produced worldwide. Papers have flourished in recent years in the attempt to describe and simulate numerically the phenomena observed in such process. To predict the solid and gas phase behavior the Eulerian-Eulerian approach has been used due to low computational effort required [2]. In this study, the Eulerian-Eulerian approach is used, where the solid phase is treated as a continuum [3–5]. Computational fluid dynamic (CFD) was implemented to solve discretized equations; a hybrid mesh (tetrahedral mesh with refining prisms at the wall) was used as the calculation grid. The 12-lump kinetic model proposed by Wu et al. [6] with catalyst deactivation was coupled with the hydrodynamic model to evaluate the full problem. The lumping approach has been studied to describe the kinetic behavior of catalytic cracking with a large number of components where each lump is constituted by hundreds of kinds of molecules in a specific range of molecular weights. The methodology is shown to be very powerful when a large number of components are involved [7–11]. The simulation model uses a 12-lump effect that the variation of different process variables has on the

conversion network which has the advantage of representing with good reliability the products and presents the option of representing the feedstock through three different lumps. The purpose of this study is to predict the yield and conversion behaviors at different operating conditions in the industrial riser of a FCC unit, with a 12-lump kinetic model. Different operational conditions have been studied, in order to estimate product yields.

2. Riser Process

The riser is the main equipment of the FCC unit. Inside the riser the feedstock is fed through nozzles and mixture with the catalyst and the accelerant steam in the injection zone. The performance of the nozzles to guarantee fast vaporization of the feedstock and a good contact of the gasoil droplets with the catalyst is key to improve the FCC riser efficiency; the feedstock nozzles are positioned about 5–12 meters above the bottom of the reactor. In accordance with kind of FCC design, the number of feedstock injections can be from 1 to 15. Practically all of the riser reactions take place between 1 and 3 s. Reactions start as soon as the feed enters in contact with the hot catalyst.

The increasing velocity due to the vapor production acts as the means to carry the catalyst up in the riser. The hot solid supplies the necessary heat to vaporize the feedstock and bring its temperature to the temperature needed for cracking, compensating, also, for the reducing in temperature due to endothermic behavior of riser reactions. Standard risers are designed for an outlet velocity of 12–18 m/s. During the operation, coke deposits on the catalyst, declining the catalyst activity and thus representing a concern for the efficiency of the cracking reactions [12].

3. Mathematical Model

The fluid dynamic equations and kinetic model are summarized in Section 3.1 and taken and adapted from Alvarez-Castro [13]; the catalytic cracking kinetic models are taken from Wu et al. [6] and Chang et al. [14]. In order to study the heterogeneous, kinetics, and the particle phase deactivation, (15)–(20) were implemented in the CFX code.

3.1. Governing Equations for Transient Two Fluid Models

Governing Equations.

(1) Gas-solid fluid model (Eulerian-Eulerian) [15]:

$$\frac{\partial}{\partial t}\left(\varepsilon_g \rho_g\right) + \nabla \cdot \left(\varepsilon_g \rho_g \mathbf{u}_g\right) = 0,$$
$$\frac{\partial}{\partial t}\left(\varepsilon_s \rho_s\right) + \nabla \cdot \left(\varepsilon_s \rho_s \mathbf{u}_s\right) = 0,$$

(1)

where ε is the volume fraction, ρ is density, and $\mathbf{u}$ is the velocity for each phase.

(2) Momentum equations:

$$\frac{\partial}{\partial t}\left(\varepsilon_g \rho_g \mathbf{u}_g\right) + \nabla \cdot \left(\varepsilon_g \rho_g \mathbf{u}_g \mathbf{u}_g\right)$$
$$= \nabla \cdot \left[\varepsilon_g \mu_g \left(\nabla \mathbf{u}_g + \left(\nabla \mathbf{u}_g\right)^T\right)\right] + \varepsilon_g \rho_g \mathbf{g} - \varepsilon_g \nabla p + M,$$
$$\frac{\partial}{\partial t}\left(\varepsilon_g \rho_g \mathbf{u}_s\right) + \nabla \cdot \left(\varepsilon_s \rho_s \mathbf{u}_s \mathbf{u}_s\right)$$
$$= \nabla \cdot \left[\varepsilon_s \mu_s \left(\nabla \mathbf{u}_s + \left(\nabla \mathbf{u}_s\right)^T\right)\right] + \varepsilon_s \rho_s \mathbf{g} - \varepsilon_s G \nabla \varepsilon_s - M,$$

(2)

where p is the pressure, μ the viscosity, G the modulus of elasticity, g the acceleration of gravity, and M the interphase momentum transfer:

$$M = \left(150 \frac{\varepsilon_s^2 \mu_g}{\varepsilon_g d_s^2} + \frac{7}{4} \frac{\left|\mathbf{u}_s - \mathbf{u}_g\right| \varepsilon_s \rho_g}{d_s}\right)\left(\mathbf{u}_s - \mathbf{u}_g\right)$$

For dense zones where, $\varepsilon_s > 0.2$,

(3)

$$M = \left(\frac{3}{4} C_d \frac{\left|\mathbf{u}_s - \mathbf{u}_g\right| \varepsilon_s \varepsilon_g \rho_g}{d_s}\right)\left(\mathbf{u}_s - \mathbf{u}_g\right)$$

For dilute zones where, $\varepsilon_s < 0.2$,

where d_s is the solid diameter and C_d is the drag coefficient

$$C_d = \frac{0.44}{\varepsilon_g^{2.65}}$$

$$\left(\text{Re} > 1000,\right.$$

adequate for inertial effects to govern viscous effects$\left.\right)$,

$$C_d = \frac{1}{\varepsilon_g^{2.65}} \frac{24}{\text{Re}}\left(1 + 0.15 \text{Re}^{0.687}\right)$$

$$\left(\text{Re} < 1000, \text{viscous and inertial effects are significant}\right),$$

$$G = \exp\left[C_G\left(\varepsilon_s - \varepsilon_{s,\max}\right)\right]$$

(4)

(see [16]), where $\varepsilon_{s,\max}$ is maximum volume fraction and the packing limited about 0.65.

(3) Turbulence equations:

$$\mu_g = \mu_{\text{lam},g} + \mu_{\text{tur},g} \quad \text{(effective viscosity)}. \quad (5)$$

(a) The k-epsilon mixture model [17]:

$$\mu_{\text{tur},g} = C_\mu \rho_g \frac{k^2}{\epsilon}, \quad (6)$$

where k is the turbulence kinetic energy, ϵ is the turbulence eddy dissipation, and C_μ is constant

$$\frac{\partial}{\partial t}\left(\rho_g k\right) + \nabla \cdot \left(\rho_g \mathbf{u}_g k\right) = \nabla \cdot \left[\mu_{\text{lam},g} + \frac{\mu_{\text{tur},g}}{\sigma_k} + \nabla k\right]$$
$$+ P^k - \rho_g \epsilon,$$
$$\frac{\partial}{\partial t}\left(\rho_g \epsilon\right) + \nabla \cdot \left(\rho_g \mathbf{u}_g \epsilon\right) = \nabla \cdot \left[\mu_{\text{lam},g} + \frac{\mu_{\text{tur},g}}{\sigma_\epsilon} + \nabla \epsilon\right]$$
$$+ \frac{\epsilon}{k}\left(C_{\epsilon,1}P^k - C_{\epsilon,2}\rho_g\epsilon\right),$$

(7)

where σ_k, σ_ϵ, $C_{\epsilon,1}$, and $C_{\epsilon,2}$ are constants. P^k is the turbulence production

$$P^k = \mu_{\text{tur},g}\left(\nabla u_g + \left(\nabla u_g\right)^T\right). \tag{8}$$

(4) Heat transfer model:

$$\frac{\partial}{\partial t}\left(\varepsilon_g \rho_g H_g\right) + \nabla \cdot \left(\varepsilon_g \rho_g u_g H_g\right)$$
$$= \nabla \cdot \left(\varepsilon_g \lambda_g \nabla T_g\right) + \gamma\left(T_s - T_g\right) \tag{9}$$
$$+ \varepsilon_g \rho_g \sum_r \nabla H_r \frac{\delta C_r}{\delta t} - Q_R - Q_V,$$

$$\frac{\partial}{\partial t}\left(\varepsilon_s \rho_s H_s\right) + \nabla \cdot \left(\varepsilon_s \rho_s u_s H_s\right) = \nabla \cdot \left(\varepsilon_s \lambda_s \nabla T_s\right) + \gamma\left(T_g - T_s\right), \tag{10}$$

where H is enthalpy, T temperature, λ thermal conductivity, Q_R heat of cracking reactions, and Q_V energy lost in gasoil vaporization

$$\gamma = \frac{\text{Nu}\lambda}{d_s}, \tag{11}$$

where γ is the interphase heat transfer coefficient, d_s is the diameter of the catalyst, and Nu is the Nusselt number

$$\text{Nu} = 2 + 0.6\sqrt{\text{Re}}\text{Pr}^{0.3} \tag{12}$$

(see [18]).

(5) Energy lost in gasoil vaporization transfer by hot solid:

$$Q_V = 400\,\text{kJ/kg of gasoil} \tag{13}$$

(see [5]).

(6) Kinetic model [6].

Variation of the chemical species:

$$\frac{\partial}{\partial t}\left(\varepsilon_g \rho_g C_{g,I}\right) + \nabla \cdot \left(\varepsilon_g \rho_g u_g C_{g,I}\right) = \nabla \cdot \left(\varepsilon_g \Gamma_i \nabla C_{g,I}\right) + \widehat{R}_I, \tag{14}$$

where Γ is diffusivity, $C_{g,I}$ is the concentration of species I in the gas phase, and $\widehat{R}_I$ is consumption or formation of each species.

(6.1) The rate equation for the generic reaction:

$$\widehat{R}_{I,r} = -k_r \cdot \rho_p \cdot (\rho\alpha_i) \cdot \phi(t) \cdot F(N) \cdot F(A), \tag{15}$$

where we have the following: $\phi(t)$, catalyst poisoning due to coke content, $F(N)$, alkaline nitrides, $F(A)$, polycyclic aromatic adsorption, k_r, kinetic constant, ρ_p, particle density, and $(\rho\alpha_i)$, the mass content of species i in gaseous phase.

(a) Decay model based on coke content:

$$\Phi(t) = e^{(-\alpha t)}, \tag{16}$$

where we have (t), time, and α, constant.

(b) Alkaline nitrides:

$$F(N) = \frac{1}{1 + k_N C_N t_C / F_{c/o}}, \tag{17}$$

where k_N is the adsorption factors of nitrides, C_N the mass content of nitrides, t_C the relative detention time of catalyst, $F_{c/o}$ the catalyst-to-oil ratio in the feedstock.

(c) Polycyclic aromatic adsorption:

$$F(A) = \frac{1}{1 + k_A (C_A + C_R)}, \tag{18}$$

where k_A is the adsorption factor of aromatics, C_A the mass content of aromatics, and C_R the mass content of resins in the feedstock.

(d) Arrhenius' equation:

$$k_r = k_r^0 \exp\left(\frac{E_r}{RT}\right). \tag{19}$$

(e) Arrhenius equation for any temperature, dependent on the holdup of solids:

$$k_c(T, \varepsilon_s) = k_{r,550°C}(\rho, \varepsilon_s)\exp\left[-\frac{E_r}{R}\left(\frac{1}{T} - \frac{1}{550°C}\right)\right]. \tag{20}$$

4. Simulation

The system of governing equations, twelve-lump catalytic cracking kinetic model, solid influence, and catalyst deactivation functions was solved by employing the finite volume method technique using the commercial software ANSYS CFX 14.0. The relevant results and the calculations steps are analyzed and discussed in detail in the following sections.
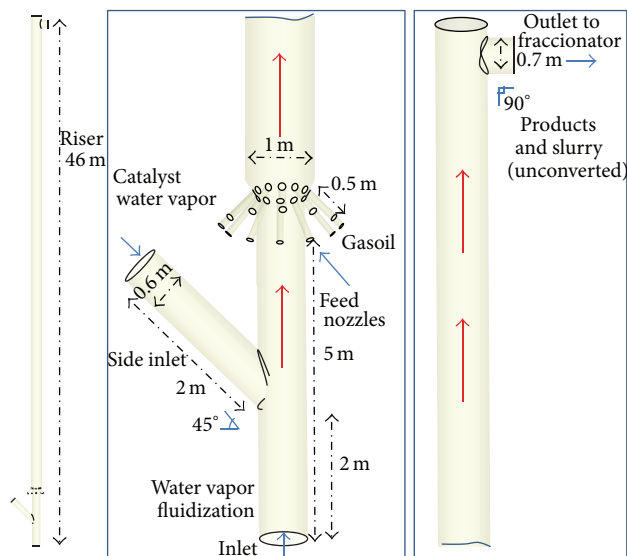
FIGURE 1: Riser geometry.

FIGURE 2: Mesh details.

TABLE 1: Operating conditions.

Item	Value
Reaction temperature (K)	793.15
Reaction time (s)	3.22
Flux of fresh feedstock (t/h)	124.46
Inlet temperature of fresh feedstock (K)	543.15
Catalyst temperature at riser inlet (K)	913.15
Ratio of catalyst to oil	8.1

4.1. Geometry and Grids Generation. Steam or fuel gas is often used to lift the catalyst to the feed injection. In most designs that incorporate a "Wye" section for delivering the catalyst to the feed nozzles, a lift gas distributor is used, providing sufficient gas for delivery of dense catalyst to the feed nozzles. In other designs, the lift gas rate is several magnitudes greater, with the intent of contacting the gasoil feed into a more dilute catalyst stream. In this work the geometry of the riser is considered according to industrial reactor specifications taken from Alvarez-Castro [13] as shown in Figure 1 which reports a typical riser with Wye section.

The geometries considered are meshed according to the procedure described above; previous works [4, 19] showed that the CFD utilized there and adopted in this work is mesh independent and meshes of 700 to 900 thousand control elements are recommended for a good representation of industrial risers. A hybrid mesh with 800 thousand control elements was built and applied in this work. Details of outlet and inlet mesh can be seen in Figure 2.

4.2. Model Setting-Up. To implement the numerical simulation, the hydrodynamic configuration of the model was set up first and then the 12-lump kinetic model was linked with the hydrodynamic equations. Appropriate specific subroutines, that is, user defined function (UDF), were implemented in the model and solved in the CFX code in order to consider the heterogeneous, endothermic kinetics and catalyst deactivation.

4.2.1. Hydrodynamic Setup. The setup considered in this work considered steam as the fluidization agent which was fed into the bottom of the riser; a side inlet was used for feeding in the particle phase. A small amount of the steam (3 to 7 wt. % of the total steam) was fed together with the catalyst and 12 nozzles, 5 meters above the riser base, were used to feed gasoil; the zone where the nozzles are located is a
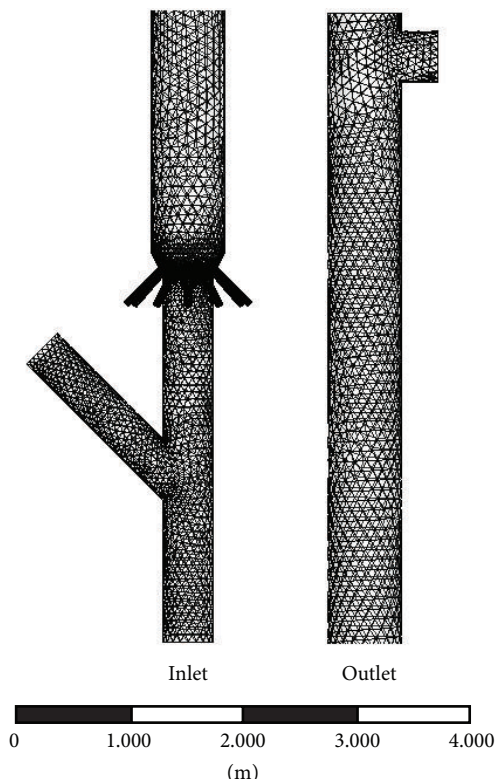
very significant one since it is responsible for guaranteeing fast vaporization of the liquid gasoil; recent technologies have led to development of high-efficient nozzles [20–22], which implies a time for complete vaporization of about 3% (around 0.05 to 0.2 seconds) of the total reactant residence time in the reactor, in typical operation conditions. In the present simulation it was assumed that the feedstock is totally vaporized. The nonslip and free slip condition at the walls was used for the phases.

Gasoil properties and operating conditions used in the present work were taken from Wu et al. [6] and Chang et al. [14] and are summarized in Tables 1 and 2, respectively.

According to Nayak et al. [5], 400 kJ/kg is the heat to be adopted in the simulation needed for the evaporation of the liquid droplets.

4.2.2. Kinetic Model Setup. A 12-lump model was used to represent the products and feedstock behavior [23]. Such model can undergo a large number of reactions (56 reactions)

Table 2: The property of feedstock.

Item	Valor
Density (kg/m^3 at 293.15 K)	924
Hydrogen content (wt%)	12.1
Group analysis (wt%)	
Saturates	66.05
Aromatics	25.25
Resins + asphaltenes	8.7
Distillation (K)	
HK	<578.15
10%	664.15
30%	709.15
50%	734.15
70%	771.15
Alkaline nitrides content (mg/g)	1750
Conradson carbon residue (wt%)	2.33

Table 3: Lumps of the 12-lump kinetic model [6].

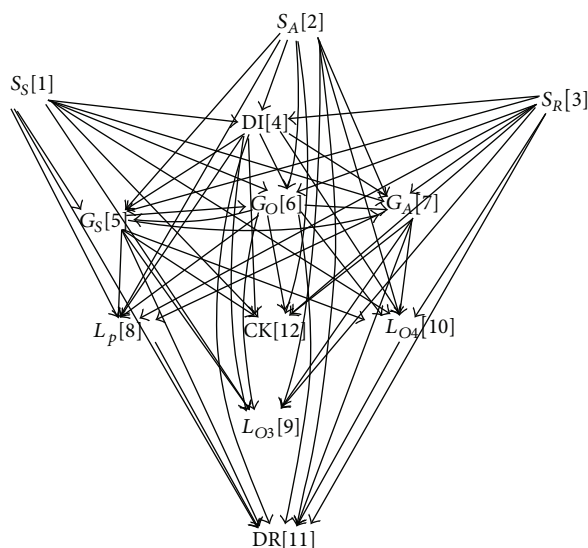| Lump symbol	Lump	Boiling range
S_S	Saturates in feedstock	613.15 K+
S_A	Aromatics in feedstock	
S_R	Resin and asphaltene in feedstock	
D_I	Diesel without pretreating LCO	477.15–613.15 K
G_S	Saturates in gasoline	C5 - 477.15 K
G_O	Olefins in gasoline	
G_A	Aromatics in gasoline	
L_P	low carbon alkanes	C3 + C4
L_{O3}	Propylene	
L_{O4}	Butene	
D_R	Dry gas	C1 + C2 + H2
C_K	Coke	

Figure 3: Twelve-lump kinetic model network [6].

leading to a large number of products depending on the different types of feedstock. The kinetic paths are shown in Figure 3 and Table 3 summarizes the different ranges of products and the feedstock characterization. The values of the kinetic constants, activation energies, and catalyst deactivation constant are listed in Table 4. In heat transfer model (9), Q_R is estimated by the amount of coke produced in cracking reactions; this factor Q_R is equal to 9.127103 kJ multiplied by the mass of coke which is corresponding to endothermic reactions in riser of FCC [6, 23].

4.3. Convergence. Transient expressions were estimated via the second-order backward Euler method. The convective terms were interpolated through a second-order upwind scheme "high-resolution method."

In the simulation was used a time step of 10^{-3} seconds to provide a lower Courant number in order to ensure simulation results were not dependent on the time step selected and monitoring the simulation with Courant number less than one. The convergence for progressing in time implied a residual square mean less than 10^{-4}. The simulations were solved using computers provided with Xeon 3 GHz dual core processors. About twelve days of calculation was necessary to predict a period of time (15 [s]) long enough to show that the variables had a cyclic behavior.

The following section reports the numerical results aimed at evaluating how the variation of the different operation variables affects the heat transfer, the chemical reaction, and the hydrodynamic behavior of the riser.

5. Results and Discussion

Comparing model predictions for industrial reactors with plant data is not an easy task because the computational model requires detailed information about the feedstock as well as the design and operating conditions of the industrial setups and petroleum companies normally do not release these data on industrial risers.

5.1. Validation of the Simulation Results. The catalyst distribution profile for the riser is shown in Figure 4. Figure 4(a) shows a rendering of volume for catalyst volume fractions along an axial extension for the first six meters of the riser height where it can be seen that, just after the expansion zone and the nozzles, the feedstock has reacted and consequently is produced and the gas velocity increases due to less products density, so the catalyst moves at the high velocities imposed by the gasoil injection and its distribution becomes increasingly uniform with increasing height. Catalyst distribution is shown on eight radial contour planes in an axial direction in Figure 4(b). On the first radial planes it can be observed that, just after expansion, the solid phase (dense region) tends to agglomerate at the center of riser. This is due to the high velocity of the injected gasoil, which prevents the phenomenon of catalyst agglomeration on the walls known as

TABLE 4: Kinetics constants and activation energies of reaction [6, 14].

Reaction path	Activation energy (kJ/mol)	Exponential factor (m^3/kg/s)	Reaction path	Activation energy (kJ/mol)	Exponential factor (m^3/kg/s)
1 → 4	2.7251	0.5496	4 → 6	13.0832	0.00785
1 → 5	0.9432	0.1478	4 → 7	12.2401	0.04245
1 → 6	1.2912	0.728	4 → 8	8.2513	0.00853
1 → 7	7.2956	0.01707	4 → 9	3.7156	0.00294
1 → 8	13.0682	0.00221	4 → 10	3.4688	0.00479
1 → 9	8.9495	0.00824	4 → 11	16.3068	0.00765
1 → 10	7.787	0.00289	4 → 12	10.2884	0.06204
1 → 11	8.8766	0.02903	5 → 6	14.641	0.01914
1 → 12	9.5764	0.02268	5 → 7	15.7166	0.00595
2 → 4	4.7964	0.5068	5 → 8	15.3998	$1.06E - 05$
2 → 5	4.0451	0.09092	5 → 9	13.124	0.00982
2 → 6	14.1004	0.0178	5 → 10	12.8934	0.04039
2 → 7	13.5735	0.02794	5 → 11	18.2895	0.00547
2 → 8	0.7088	0.03926	5 → 12	19.805	0.00055
2 → 9	3.4203	0.0579	6 → 5	12.6572	0.06655
2 → 10	3.7921	0.02698	6 → 7	8.9658	0.1029
2 → 11	4.7483	0.02206	6 → 8	13.5233	$1.25E - 13$
2 → 12	3.3867	0.04335	6 → 9	12.1083	0.0297
3 → 4	10.1081	0.04164	6 → 10	12.1945	0.0246
3 → 5	14.3479	0.02781	6 → 11	14.6554	0.01485
3 → 6	15.8237	0.1043	6 → 12	11.3696	0.00878
3 → 7	16.01057	0.01088	7 → 8	14.0169	$1.30E - 06$
3 → 8	0.9537	0.3375	7 → 9	11.9348	0.01566
3 → 9	1.9214	0.1208	7 → 10	10.4221	0.08629
3 → 10	1.35212	0.08769	7 → 11	10.2512	0.09008
3 → 11	4.0009	0.05663	7 → 12	9.3636	0.05506
3 → 12	3.9143	0.06459	8 → 11	30.3051	0.002563
4 → 5	14.4455	0.006942	10 → 11	38.5004	0.000683
$k_A = 0.003854$		$k_N = 0.002009$		$\alpha = 0.002543$	

coral annulus and guarantees keeping a much more uniform distribution (better homogenization) throughout the riser.

The fluidization velocity of the steam, at the bottom of the equipment, has a major effect on catalyst residence time in the reaction system as presented in previous work by Alvarez-Castro [13].

The model developed for the riser simulation was used to simulate the plant data reported by Chang et al. [14], in order to validate the model and compare the product yields and conversions behavior. Products distributions, that is, the average yields, along the height of the riser are shown in Figure 5. Red and green curves represent the main yield products (gasoline and diesel, resp.); it can be seen that after 25 meters an asymptotic behavior is achieved at the end of the equipment, with less conversion, due to overcracking. Blue, yellow, and brown curves represent LPG, dry gas, and coke, respectively. The black curve shows the total unconverted slurry. Results show good agreement between simulation and experimental data.

Conversions and final products yields simulations model and the industrial data are shown in Figures 6 and 7, respectively. Measurements were taken at the riser outlet in order to compare the accuracy of the model simulation with the predicted results.

5.2. Operational Variables. Data obtained from Petrobras on the multipurpose pilot unit U-144 (height of 17 m and diameter of 0.52 m) in which different tests were carried out by changing the feedstock temperature, the catalyst temperature, and the catalyst-to-oil ratio are reported in Table 5.

The sensitivity of the conversions and products yields to process variables, based on the validated simulation model, was studied. The conversions and yields were found to be very sensitive to variations in feedstock temperature, catalyst temperature, and catalyst-to-oil ratio; the differences in the conversion and product yields were in the range of 1% to 5%.

TABLE 5: General behavior of the multipurpose pilot unit U-144 studied.

Item	Catalyst to oil ratio 7.8 to 8.6	Catalyst temperature 680 to 720 (K)	Temperature of fresh feedstock 530 to 550 (K)	Residence time 1 to 2.2 [s]
Slurry (unconverted)	Decrease	Decrease	Decrease	Decrease
DI diesel	Decrease	Decrease	Decrease	Decrease
Gasoline	Decrease	Decrease	Decrease	Decrease
LPG	Increase	Increase	Increase	Increase
DR dry gas	Increase	Increase	Increase	Increase
CK coke	Increase	Increase	Increase	Increase

(a)   (b)
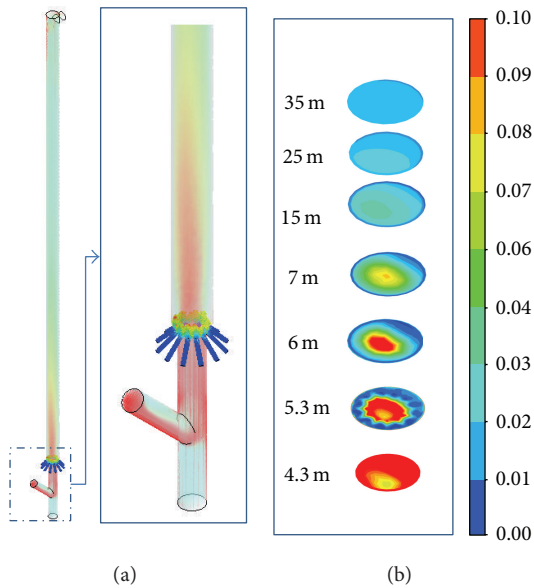
FIGURE 4: Volume rendering and contour profiles for axial and radial planes of catalyst volume fractions.
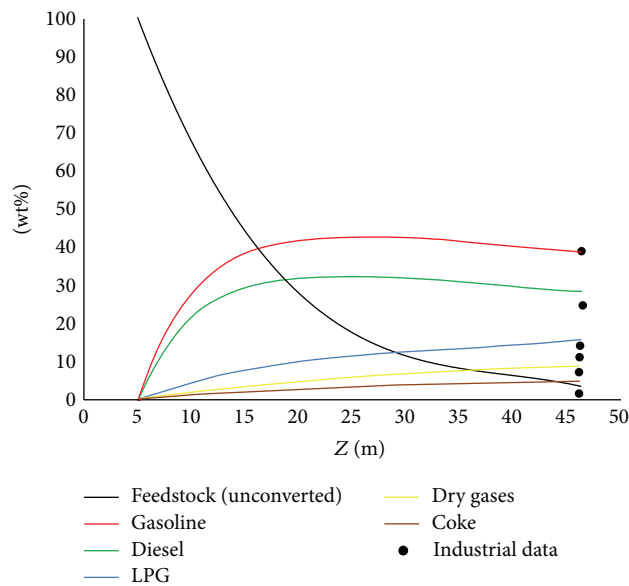

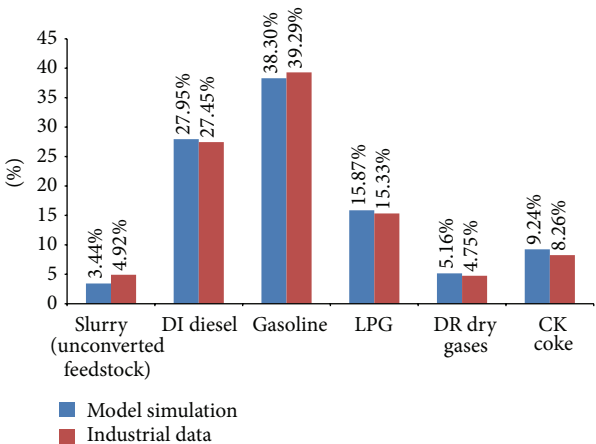FIGURE 5: Model simulation results and industrial data.

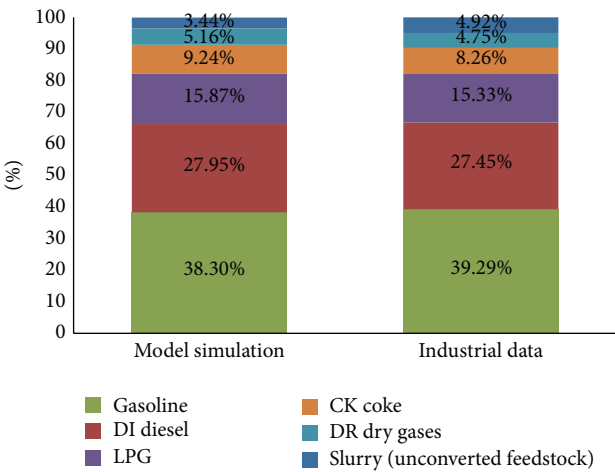FIGURE 6: Comparison between product yields industrial data and the simulation model.

FIGURE 7: Comparison between industrial data and the simulation model for each case.

Followed, results obtained for the three variables studied in this order:

(a) feedstock temperature,

(b) catalyst temperature,

(c) catalyst-to-oil ratio.

TABLE 6: Operating conditions with variations in feedstock temperature.

Item	Case A Value	Case B Value	Case C Value	Case D Value	Case E Value
Reaction temperature (K)	793.15	793.15	793.15	793.15	793.15
Fluidization steam (%)	3	3	3	3	3
Flux of fresh feedstock (t/h)	124.46	124.46	124.46	124.46	124.46
Inlet temperature of fresh feedstock (K)	**443.15**	**493.15**	**543.15**	**593.15**	**643.15**
Catalyst temperature at riser inlet (K)	913.15	913.15	913.15	913.15	913.15
Ratio of catalyst to oil	8.1	8.1	8.1	8.1	8.1

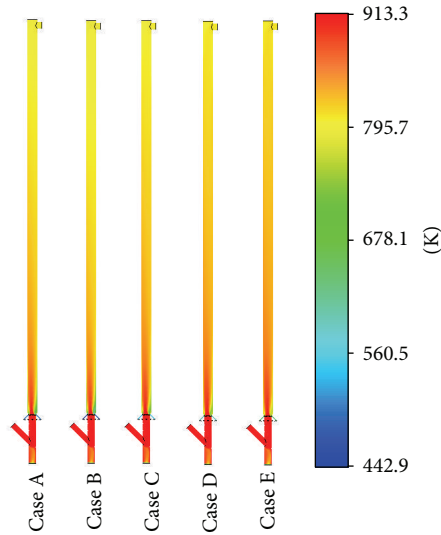FIGURE 8: Temperature profiles for the axial plane with variation feedstock temperature.

FIGURE 9: Temperature profiles through riser with variation in feedstock temperature.

5.2.1. Feedstock Temperature.

Different case studies for temperatures ranging between 443.15 K and 643.15 K were tested while holding the other operating conditions constant, as shown in Table 6.

(1) Comparison of the Hydrodynamics Profiles for Different Feedstock Temperatures. The global temperature (two phases) was calculated as arithmetic average contour planes for all the case studies as shown in Figure 8; the profile for case A has the lowest inlet feedstock temperature and profile for case E has the highest. It can be observed that the temperature distributions are similar in all cases with an approximate variation of 50 [K] between the first and last cases A and E.

Figure 9 contains the profiles for average temperature (two phases) along the center line of riser height which was also calculated as arithmetic average; the temperature decreases significantly after the feeding area, due to the endothermic nature of the reaction.

(2) Dependence of Product Yield on Feedstock Temperature. The percentage of yield and conversion products for each case presented in the previous section is shown in Figure 10. The yields were broken down into the following main groups: gasoline, diesel, LPG, dry gas, and coke. Feedstock cracking is
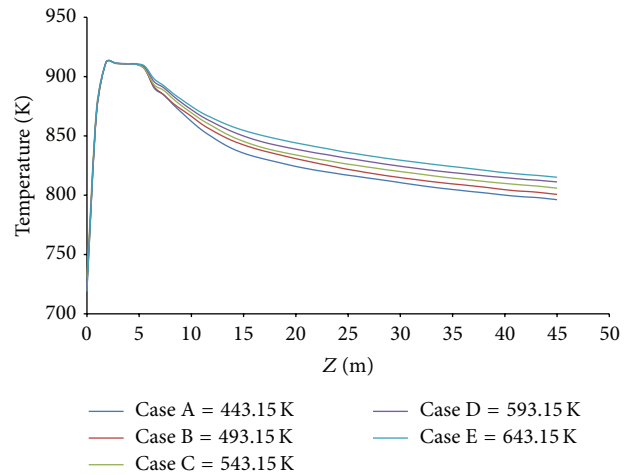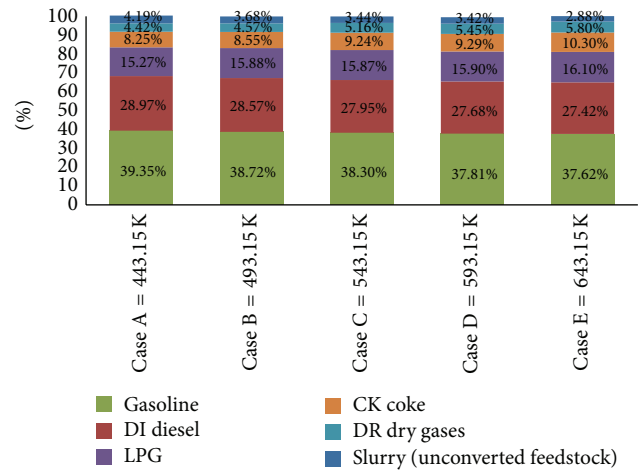

FIGURE 10: Products yields for each feedstock temperature.

represented by complex series-parallel reactions where gasoline and diesel are intermediate products from which the final products (LPG, dry gas, and coke) are produced. If feedstock rate of conversion is too high because of high temperature, the secondary reactions of the intermediate products cause the rate of yield to decrease due to overcracking or generation of more final products.

TABLE 7: Operating conditions with variations in catalyst temperature.

Item	Case A Value	Case B Value	Case C Value	Case D Value	Case E Value
Reaction temperature (K)	793.15	793.15	793.15	793.15	793.15
Fluidization steam (%)	3	3	3	3	3
Flux of fresh feedstock (t/h)	124.46	124.46	124.46	124.46	124.46
Inlet temperature of fresh feedstock (K)	543.15	543.15	543.15	543.15	543.15
Catalyst temperature at riser inlet (K)	**813.15**	**863.15**	**913.15**	**963.15**	**1013.15**
Ratio of catalyst to oil	8.1	8.1	8.1	8.1	8.1
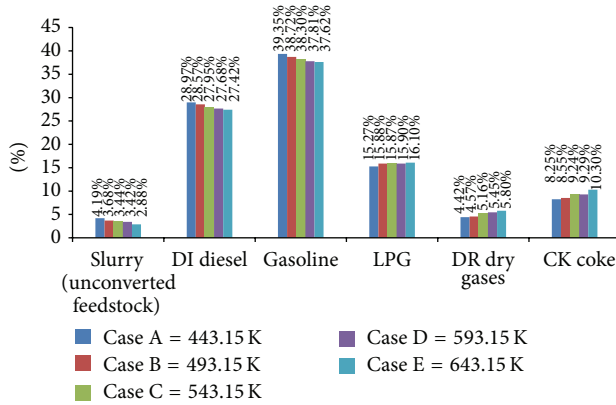
FIGURE 11: Comparison of the product yields for different feedstock temperatures.

FIGURE 12: Global temperature profiles for the axial plane with variations in catalyst temperature.

Feedstock temperature has an important role in the process. A comparison of the product yields and conversion for all cases studied is reported in Figure 11, where it can be seen that cases A, B, and C have higher gasoline and diesel yields but a lower feedstock conversions, while cases D and E have lower gasoline and diesel yields but a higher diesel conversion. The temperature is lower at the higher gasoline and diesel yields, the importance of which should be evaluated by a cost analysis of feedstock reprocessing or production of dry gases and coke in order to improve the plant targets.

5.2.2. Catalyst Temperature. Different cases with catalyst temperatures ranging between 813.15 [K] and 1013.15 [K] were tested while holding constant the other operating conditions as shown in Table 7.

(1) The Effect of Catalyst Temperature on Riser Hydrodynamics. The global temperature (gas and solid) was calculated as arithmetic average contour planes for the different case studies are shown in Figure 12. Case A is characterized by lower average overall temperature in the riser, while cases B, C, D, and E show a drastic increase in the average overall temperature in the riser with higher temperature in the profile for case E. It may be noted that small changes in the catalyst feed temperature cause a significant increase in the overall temperature.

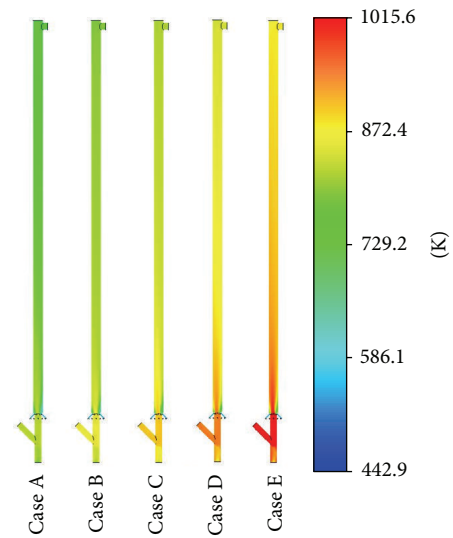Temperature profiles plotted along the riser height are shown in Figure 13 for all cases studied and were calculated as arithmetic average (gas and solid phases). It can be observed that catalyst temperature has a strong effect on the overall temperature in the riser, showing that the temperature profiles with a variation of 50 [K] similar to the inlet temperature of the catalyst have a much greater effect.

(2) Dependence of Product Yields on Catalyst Temperature. The percentages of conversions and product yields for each case studied are shown in Figure 14. The percentages of converted gasoil and product yields are reported.

The product yields for each case studied are shown in Figure 15. Case A has higher gasoline and diesel yields but a lower conversion of diesel, while case E has lower gasoline and diesel yields and a higher percentage of final products such as light gases, coke, and LPG. In the latter case the feedstock conversion is higher due to the higher temperature, which causes the intermediates to undergo overcracking generating lighter products of lower commercial value.

5.2.3. Catalyst-to-Oil Ratio Study. Catalyst-to-oil ratios from 6.1 to 10.1, with step increases ratio of 1 for all cases, were studied while holding all other variables constant as shown in Table 8.

TABLE 8: Operating conditions with variations in catalyst-to-oil ratio.

| Item	Case A Value	Case B Value	Case C Value	Case D Value	Case E Value
Reaction temperature (K)	793.15	793.15	793.15	793.15	793.15
Fluidization steam (%)	3	3	3	3	3
Flux of fresh feedstock (t/h)	124.46	124.46	124.46	124.46	124.46
Inlet temperature of fresh feedstock (K)	543.15	543.15	543.15	543.15	543.15
Catalyst temperature at riser inlet (K)	913.15	913.15	913.15	913.15	913.15
Ratio of catalyst to oil	**6.1**	**7.1**	**8.1**	**9.1**	**10.1**
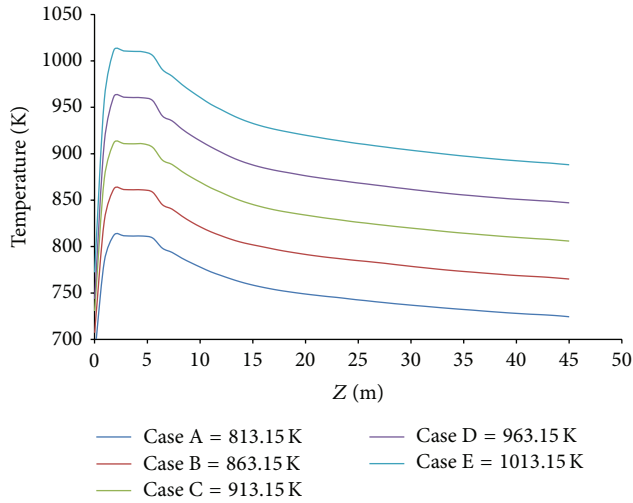
FIGURE 13: Temperature profiles through riser altering catalyst temperature profiles for the riser with variations in catalyst temperature.
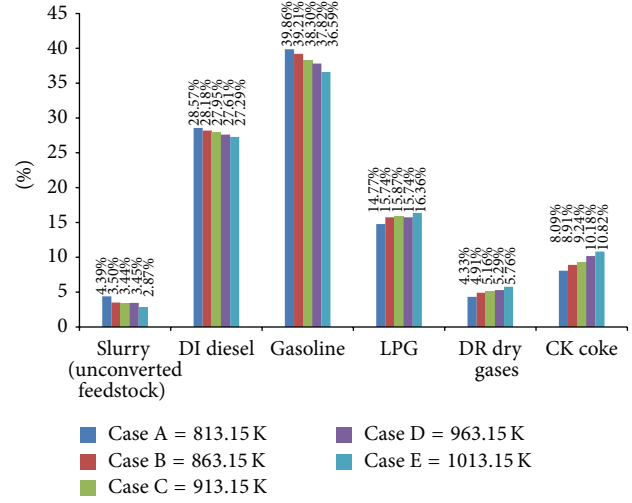

FIGURE 15: Comparison of the product yields for different catalyst temperatures.
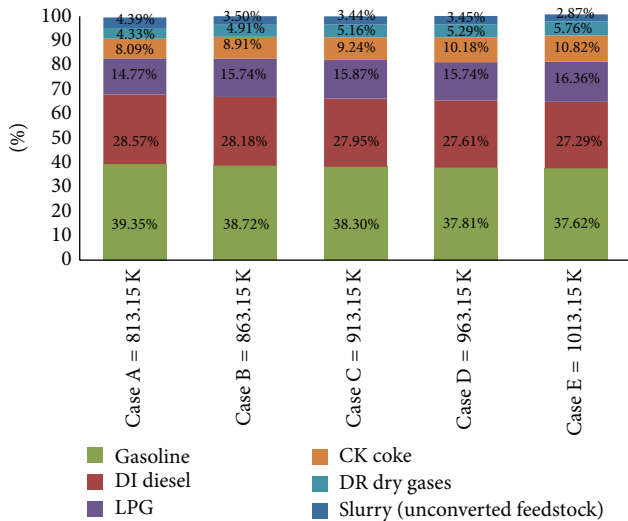

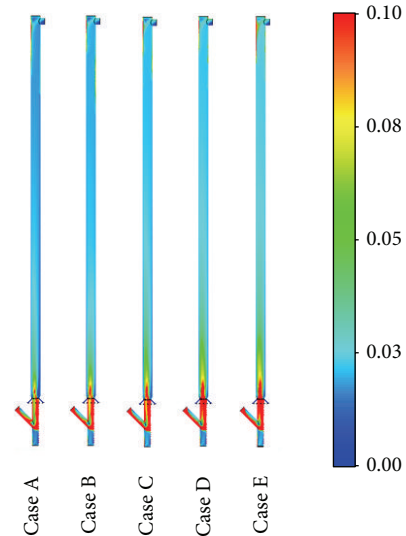FIGURE 14: Products yields for each catalyst temperature.

FIGURE 16: Catalyst volume fraction profiles for catalyst-to-oil ratio.

(1) Dependence Riser Hydrodynamics on Catalyst-to-Oil Ratio. The catalyst-to-oil ratio is an important variable, since it has a direct effect on the conversion and selectivity of gasoline and diesel. Figure 16 shows the profile of the catalyst volume

fraction for the different case studies with case A having a lower catalyst-to-oil ratio and case E having a higher one in comparison to all cases studied. In both cases A and B, it can be noted that the fraction of catalyst is lower along the riser
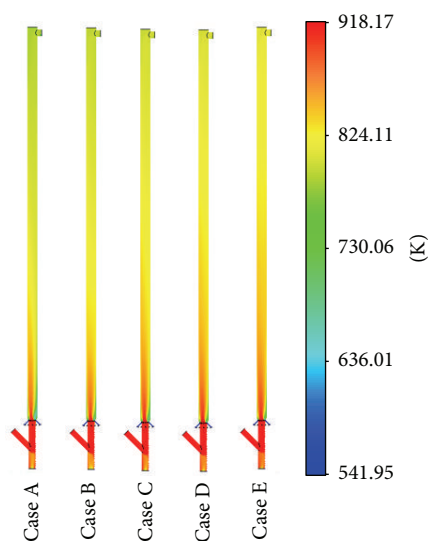
FIGURE 17: Temperature profiles for the axial plane with variations in catalyst-to-oil ratio.
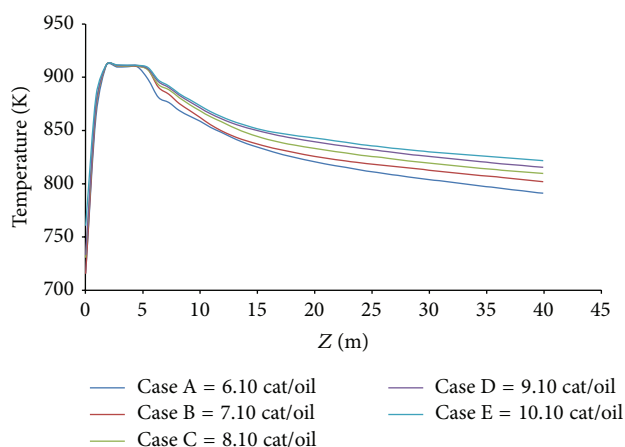

FIGURE 18: Temperature profiles for the riser with variation in catalyst-to-oil ratio.

FIGURE 19: Product yields for each catalyst-to-oil ratio.

FIGURE 20: Comparison of the product yields for catalyst-to-oil ratio.

height and higher at the side where the catalyst is fed in. In cases D and E catalyst fraction is higher and more uniform along the riser height.

At the bottom of the riser, where the feedstock is injected, the temperature profile is very complex and chaotic due to the contact between hot catalyst, reagents, and steam.

Figure 17 shows the temperature profiles for a contour plane. Case A is characterized by a lower catalyst-to-oil ratio while case E represents a higher catalyst-to-oil ratio. The temperature profiles increase from case A to case E.

Figure 18 contains the temperature global profiles (gas and solid) along the center line of the riser which can be observed with variations in catalyst-to-oil ratio. When the gas encounters the barrier formed by the catalyst particles, which begins the reaction, the temperature decreases slowly along the riser due to the endothermic nature of the reaction.
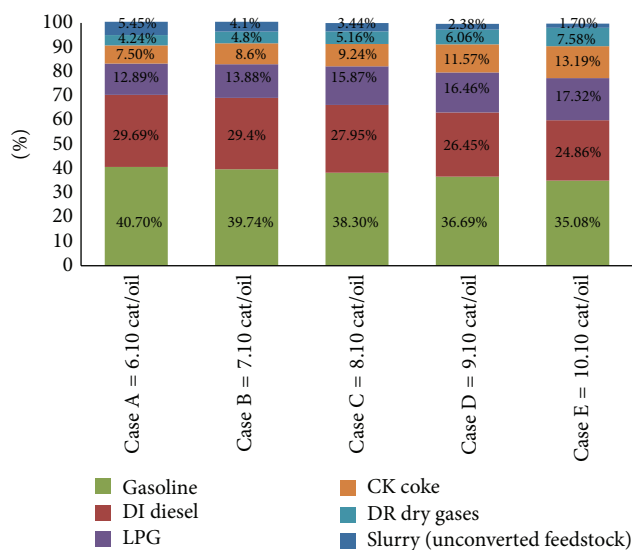
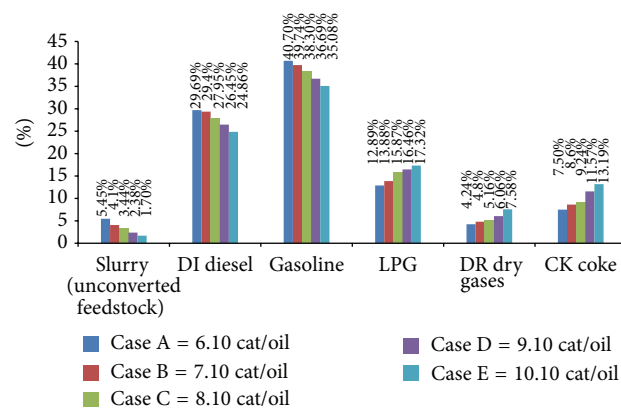*(2) Dependence of Product Yields on Catalyst-to-Oil Ratio.* The conversions and yields for each case study are reported in Figure 19 with case A characterized by a lower catalyst-to-oil ratio and case E by a higher catalyst-to-oil ratio. It can be noted that this variable has a large impact on product yield, especially for gasoline and diesel.

A comparison of the product yields in the case studied is presented in Figure 20. Case A has higher gasoline and diesel yields but a lower conversion of feedstock; on the contrary, case E, with a higher catalyst-to-oil ratio, has lower gasoline and diesel yields but higher percentages of light gases, coke, and LPG. Case A has a higher kinetic gas, but on the other hand, diesel yield is low because of a lower catalyst-to-oil ratio. Higher catalyst-to-oil ratio undergoes an overcracking, which generates lighter and lower value products.

6. Conclusions

The kinetic and hydrodynamic behavior of the riser in a FCC process has been simulated employing the 12-lump kinetics model in conjunction with ANSYS CFX 14.0 software. The model has been validated against industrial data showing the ability to capture the relevant features characterizing the industrial FCC riser behavior. Systematic investigations have been carried out to study the influence of the catalyst temperature, the feedstock temperature, and the catalyst-to-oil ratio on the riser performance. Specifically, it has been shown that when the inlet conditions (of the feedstock and catalyst) are fixed, the yield of the wanted product can be increased by controlling the temperature of the riser and the catalyst-to-oil ratio. Conditions which lead to a better homogenization of the flow, avoiding unwanted hydrodynamic features, such as the core-annulus flow, which could lead to poor conversion, have also been identified. By comparing the simulated results with the experimental data, it can be concluded that the model mimics well the process; therefore, the model can be employed as a tool helping the design, operation, and control of industrial FCC risers.

Nomenclature

C_i: Molar concentration of component I [kmol m^{-3}]
C_d: Drag coefficient [-]
C_G: Constant of elasticity modulus function [Pa]
C_μ: Constant 0.09
$C_{\epsilon,1}$: Constant 1.44
$C_{\epsilon,2}$: Constant 1.92
d: Particle diameter [m]
E: Activation energy [Jmol^{-1}]
g: Gravitational acceleration [m^{2}s^{-1}]
G: Elasticity modulus [Pa]
H: Static enthalpy [Jmol^{-1}]
k: Kinetic constant of reaction [m^{3}kmol^{-1}s^{-1}] or turbulent kinetic energy [m^{2}s^{-2}]
k^0: Preexponential factor [m^{3}kmol^{-1}s^{-1}]
k_c: Deactivation constant [kg$_{cat}$kmol^{-1}]
Nu: Nusselt number [-]
p: Static pressure [Pa]
p^k: Shear production of turbulence [Pas^{-1}]
Pr: Prandtl number [-]
q_1: Specific coke concentration [k$_{mol}$kg^{-1}$_{cat}$]
R: Reaction rate [k$_{mol}$m^{-3}s^{-1}] or universal gas constant [Jmol^{-1} K^{-1}]
Re: Reynolds number [-]
T: Static temperature [K]
u: Velocity vector [ms^{-1}]
Q_R: Heat of cracking reactions [JKg^{-1}]
Q_V: Energy lost in gasoil vaporization [JKg^{-1}].

Greek Letters

M: Interphase momentum transfer [kgm^{-3}s^{-1}]
ε: Volume fraction [-]
ϵ: Turbulence dissipation rate [m^{2}s^{-3}]
$\emptyset$: Catalyst decay function [-]
γ: Interphase heat transfer coefficient [Wm^{-2} K^{-1}]
Γ: Diffusivity [kgm^{-1}s^{-1}]
λ: Thermal conductivity [Wm^{-1} K^{-1}]
μ: Molecular viscosity [Pas]
ρ: Density [kgm^{-3}]
σ_k: Constant 1.00
σ_ϵ: Constant 3.00
$C_{\epsilon,1}$: Constant 3.00
$C_{\epsilon,2}$: Constant 3.00
φ: Tracer concentration [kg/m^3].

Subscripts

g: Gas phase
s: Solid phase
R: Reaction
lam: Laminar
turb: Turbulent.

Conflict of Interests

The authors declare that their research is only for academic purposes; there is not any financial gain or other kind of benefits influenced by secondary interest.

Acknowledgment

References

[1] R. Sadeghbeigi, "Process description," in *Fluid Catalytic Cracking Handbook*, R. Sadeghbeigi, Ed., chapter 1, pp. 1–42, Butterworth-Heinemann, Oxford, UK, 3rd edition, 2012.

[2] F. Durst, D. Milojevic, and B. Schönung, "Eulerian and Lagrangian predictions of particulate two-phase flows: a numerical study," *Applied Mathematical Modelling*, vol. 8, no. 2, pp. 101–115, 1984.

[3] X. Lan, C. Xu, G. Wang, L. Wu, and J. Gao, "CFD modeling of gas–solid flow and cracking reaction in two-stage riser FCC reactors," *Chemical Engineering Science*, vol. 64, no. 17, pp. 3847–3858, 2009.

[4] G. C. Lopes, L. M. Rosa, M. Mori, J. R. Nunhez, and W. P. Martignoni, "Three-dimensional modeling of fluid catalytic cracking industrial riser flow and reactions," *Computers and Chemical Engineering*, vol. 35, no. 11, pp. 2159–2168, 2011.

[5] S. V. Nayak, S. L. Joshi, and V. V. Ranade, "Modeling of vaporization and cracking of liquid oil injected in a gas-solid riser," *Chemical Engineering Science*, vol. 60, no. 22, pp. 6049–6066, 2005.

[6] F. Y. Wu, H. Weng, and S. Luo, "Study on lumped kinetic model for FDFCC I. Establishment of model," *China Petroleum Processing and Petrochemical Technology*, no. 2, pp. 45–52, 2008.

[7] J. Ancheyta-Juárez, F. López-Isunza, E. Aguilar-Rodríguez, and J. C. Moreno-Mayorga, "A strategy for kinetic parameter

estimation in the fluid catalytic cracking process," *Industrial & Engineering Chemistry Research*, vol. 36, no. 12, pp. 5170–5174, 1997.

[8] H. Farag, A. Blasetti, and H. de Lasa, "Catalytic cracking with FCCT loaded with tin metal traps. Adsorption constants for gas oil, gasoline, and light gases," *Industrial & Engineering Chemistry Research*, vol. 33, no. 12, pp. 3131–3140, 1994.

[9] I. Pitault, D. Nevicato, M. Forissier, and J.-R. Bernard, "Kinetic model based on a molecular description for catalytic cracking of vacuum gas oil," *Chemical Engineering Science*, vol. 49, no. 24, pp. 4249–4262, 1994.

[10] V. W. Weekman Jr., "Model of catalytic cracking conversion in fixed, moving, and fluid-bed reactors," *Industrial & Engineering Chemistry Process Design and Development*, vol. 7, no. 1, pp. 90–95, 1968.

[11] L. C. Yen, R. E. Wrench, and A. S. Ong, "Reaction kinetic correlation equation predicts fluid catalytic cracking coke yields," *Oil and Gas Journal*, vol. 86, no. 2, pp. 67–70, 1988.

[12] R. Sadeghbeigi, "Process and mechanical design guidelines for FCC equipment," in *Fluid Catalytic Cracking Handbook*, chapter 11, pp. 223–240, Butterworth-Heinemann, Oxford, UK, 3rd edition, 2012.

[13] H. C. Alvarez-Castro, *Analysis of process variables via CFD to evaluate the performance of a FCC riser [Ph.D. thesis]*, Chemical Engineering Departament, University of Campinas, 2014.

[14] J. Chang, K. Zhang, F. Meng, L. Wang, and X. Wei, "Computational investigation of hydrodynamics and cracking reaction in a heavy oil riser reactor," *Particuology*, vol. 10, no. 2, pp. 184–195, 2012.

[15] T. B. Anderson and R. Jackson, "Fluid mechanical description of fluidized beds. Equations of motion," *Industrial & Engineering Chemistry Fundamentals*, vol. 6, no. 4, pp. 527–539, 1967.

[16] D. Gidaspow, *Multiphase Flow and Fluidization: Continuum and Kinetic Theory Descriptions*, Academic Press, Boston, Mass, USA, 1994.

[17] F. R. Menter, "Two-equation eddy-viscosity turbulence models for engineering applications," *AIAA journal*, vol. 32, no. 8, pp. 1598–1605, 1994.

[18] W. E. Ranz and W. R. Marshall Jr., "Evaporation from drops, part I," *Chemical Engineering Progress*, vol. 48, pp. 141–146, 1952.

[19] H. C. Alvarez-Castro, E. M. Matos, M. Mori, and W. P. Martignoni, "3D CFD mesh configurations and turbulence models studies and their influence on the industrial risers of fluid catalytic cracking," in *Proceedings of the AIChE Spring Annual Meeting*, Pittsburgh, Pa, USA, 2012.

[20] KBR-Technology, *ATOMAX-2 Feed Nozzles*, 2009.

[21] J. Li, Z.-H. Luo, X.-Y. Lan, C.-M. Xu, and J.-S. Gao, "Numerical simulation of the turbulent gas-solid flow and reaction in a polydisperse FCC riser reactor," *Powder Technology*, vol. 237, pp. 569–580, 2013.

[22] L. M. Wolschlag and K. A. Couch, "New ceramic feed distributor offers ultimate erosion protection," *Hydrocarbon Processing*, pp. 1–25, 2010.

[23] J. Chang, F. Meng, L. Wang, K. Zhang, H. Chen, and Y. Yang, "CFD investigation of hydrodynamics, heat transfer and cracking reaction in a heavy oil riser with bottom airlift loop mixer," *Chemical Engineering Science*, vol. 78, pp. 128–143, 2012.

Journal of
Engineering

International Journal of
Rotating Machinery

The Scientific
World Journal

Journal of
Sensors

International Journal of
Distributed
Sensor Networks

Advances in
Civil Engineering

Journal of
Control Science
and Engineering

Journal of
Robotics

Journal of
Electrical and Computer
Engineering

Hindawi

Submit your manuscripts at
http://www.hindawi.com

Advances in
OptoElectronics

VLSI Design

International Journal of
Navigation and
Observation

Modelling &
Simulation
in Engineering

International Journal of
Aerospace
Engineering

International Journal of
Chemical Engineering

International Journal of
Antennas and
Propagation

Active and Passive
Electronic Components

Shock and Vibration

Advances in
Acoustics and Vibration